

MiniFool— Physics-Constraint-Aware Minimizer-Based Adversarial Attacks in Deep Neural Networks

Lucie Flek^{1,2}, Oliver Janik^{3,6}, Philipp Alexander Jung⁴, Akbar Karimi^{1,2},
 Timo Saala⁵, Alexander Schmidt⁴, Matthias Schott⁵, Philipp Soldin³,
 Matthias Thiesmeyer^{3,7}, Christopher Wiebusch³, Ulrich Willemsen⁴

¹Bonn-Aachen International Center for Information Technology, University of Bonn, 53115 Bonn, Germany.

²Lamarr Institute for Machine Learning and Artificial Intelligence, North Rhine-Westphalia, Germany.

³III. Physikalisches Institut B, RWTH Aachen University, 52056 Aachen, Germany.

⁴III. Physikalisches Institut A, RWTH Aachen University, 52056 Aachen, Germany.

⁵Physikalisches Institut, University of Bonn, 53115 Bonn, Germany.

⁶now at Erlangen Centre for Astroparticle Physics, Friedrich-Alexander-Universität Erlangen-Nürnberg, 91058 Erlangen, Germany.

⁷now at Dept. of Physics and Wisconsin IceCube Particle Astrophysics Center, University of Wisconsin—Madison, USA.

Abstract

In this paper, we present a new algorithm, **MiniFool**, that implements physics-inspired adversarial attacks for testing neural network-based classification tasks in particle and astroparticle physics. While we initially developed the algorithm for the search for astrophysical tau neutrinos with the IceCube Neutrino Observatory, we apply it to further data from other science domains, thus demonstrating its general applicability. Here, we apply the algorithm to the well-known MNIST data set and furthermore, to Open Data data from the CMS experiment at the Large Hadron Collider. The algorithm is based on minimizing a cost function that combines a χ^2 based test-statistic with the deviation from the desired target score. The test statistic quantifies the probability of the perturbations applied to the data based on the experimental uncertainties. For our studied use cases, we find that the likelihood of a flipped classification differs for both the initially correctly and incorrectly classified events. When testing changes of the classifications as a function of an attack parameter that scales the experimental uncertainties, the robustness of the network decision can be quantified. Furthermore, this allows testing the robustness of the classification of unlabeled experimental data.

Keywords: Adversarial Attacks, Artificial Intelligence, CMS, IceCube, Machine Learning, **MiniFool**

1 Introduction

In recent decades, machine learning-based algorithms have become a central cornerstone of data analysis in particle and astroparticle physics [1]. Many current results have become possible because of the use of deep neural networks in classification and regression tasks. Prime examples are several recent discoveries from the IceCube Neutrino observatory [2–4] as well as unprecedented composition measurements from the Pierre Auger Observatory [5], and enhanced detector simulations of complex detectors at the Large Hadron Collider (LHC) [6–8].

Given the importance of enhanced precision in data analysis, understanding network decisions and their robustness with respect to subtle changes of the input becomes highly important. It is well-known in machine learning that adversarial attacks that modify the input with imperceptible perturbations can drastically change the output of networks [9]. This is highly relevant for the safety of networks in commercial and financial applications. However, for particle physics applications, adversarial attacks turn out to be valuable tools as well. Here, one often considers classification tasks, where neural networks split a data set of discretely recorded events into signal and background.

The training is usually based on labeled Monte Carlo simulations of such events [10]. Subtle mismodeling of the experimental instruments can cause the networks to learn features that might not be real, therefore degrading the classification performance, once applied to the experimental data. This degradation is difficult to quantify or might not even be recognized. In view of these challenges, the application of adversarial attacks as a tool allows not only for testing the robustness of network decisions [11] but also enables the improvement of the robustness itself by specifically training the networks with adversarially attacked data [12].

In this paper, we present a new algorithm, **MiniFool**, that has been developed in the context of the search for astrophysical tau neutrinos [2] in the IceCube Neutrino Observatory [13]. Most well-known attack algorithms in the literature focus on perturbing the input data in a minimal way, but they often do not obey experimental uncertainties or boundary conditions, such as conservation laws of physics or non-physical data values, such as negative signals. Even when supplementing the attack algorithm with additional boundary constraints, the minimal change in data that leads to a change in classification might not represent a data event within the physically allowed phase space. Consequently, the statistical and physical interpretation of the success rate of attacks is difficult.

On the contrary, the approach of **MiniFool** is to optimize the attack also with respect to physically reasonable changes. This is based on the minimization of a cost function that balances the required change of the target score with the required change of the input. This change is quantified by the mean square difference relative to the physical uncertainty of the data. As a result, we can use the success rate of the attack to assess the robustness of the network. If the perturbation of an attack that is required to reach a changed target classification becomes too costly with respect to the data uncertainties, **MiniFool** will not change the classification.

In this paper, we start by briefly reviewing existing attack algorithms and their respective difficulty when applying them to our use cases. The underlying test statistic of **MiniFool** is motivated next. We then present the results for an initial example case, where we apply the algorithm to the MNIST data set [14, 15] — a well-known classification challenge in the literature. We then turn to the identification of tau neutrinos in IceCube [2], the context within which this algorithm was developed. Finally, we study the event classification of b-quark-jets using CMS open data from the Large Hadron Collider [16]. Here we see that the algorithm is generalizable to other particle physics examples. The paper ends with a discussion of the results.

2 Related Work

Adversarial attacks have been studied for more than a decade and are evolving as a valuable tool in astroparticle and elementary particle physics (See e.g. [17–19]). Several established adversarial attacks have been tested in those fields. A very well-known method is the *Fast Gradient Sign Method (FGSM)* [12]. The algorithm evaluates the signed gradient of the cost function with respect to the input data for constructing a minimally perturbed input. Smaller perturbations can be achieved with the *Projected Gradient Descent (PGD)* [20] or the *DeepFool* algorithm [21]. These can be understood as iterative extensions of the FGSM algorithm that more efficiently find a minimally perturbed solution to a changed classification. Used norms for the cost function vary between L_∞ , L_2 , and L_1 .

This approach makes these algorithms particularly well-suited for generating adversarial examples with changes that are imperceptible to human perception. However, what is common in the aforementioned algorithms is that these minimal perturbations of the input data are not constrained, and non-physical or negative pixel values are possible, if this improves the solution. Unless the algorithms are supplemented with countermeasures by additional constraints on the ranges of possible changes of the input data (See e.g. [22]), the applicability to classification tasks in particle physics analyses is limited.

The approach of **MiniFool** is different. Instead of minimizing the distance metric to the decision boundary, the cost function of perturbations includes a distance metric that quantifies the credibility of perturbations given by the uncertainties of the input data. By this, we minimize the perturbation with respect to maximum plausibility. A very similar approach has been found in the L-BFGS algorithm by Szegedy et al. [23] where they minimize a scaled distance-metric $\|\vec{r}\|_2$ of the unperturbed \vec{x} and perturbed $\vec{x} + \vec{r}$ input plus a loss term f that depends on the perturbed data and the cross-entropy loss of the targeted classification label l

$$\min_{\vec{r}} [s \cdot \|\vec{r}\|_2 + f(\vec{x} + \vec{r}, l)]. \quad (1)$$

This minimization is performed iteratively with different parameters $s > 0$ to find a global optimum of minimum distance. This concept is adopted by Carlini et al. [11], where different loss functions f are used for evaluating the robustness of network classifications. In our approach, we deviate from a simple scale parameter s but add physical uncertainties to the distance metrics. The scale of the attack s is applied to these uncertainties. Furthermore, instead of evaluating the loss function of the network, we replace it with a statistically motivated L_2 distance metric of the perturbed output and a targeted label score.

3 Minimizer-Based Network Perturbations

In this work, we restrict ourselves to a classification task with m classes. This means that the network output $\vec{f}(\vec{x}; \vec{\theta})$ is a vector of dimension m which is a non-linear function of the input data \vec{x} . Here $\vec{\theta}$ are the hidden parameters of the network. It is very common to use a softmax activation function in the final output layer, which results in output data that can be interpreted such that the value $f_i \in \vec{f}$ is the probability of the input belonging to class $i \in m$. The loss function during training is usually the cross-entropy and the maximum

$$i^* = \arg \max_i f_i(\vec{x}; \vec{\theta}) \quad (2)$$

becomes the assigned class. The goal of adversarial perturbations is to change the original input \vec{x}^0 to \vec{x}^a such that the output becomes

$$\arg \max_i f_i(\vec{x}^a; \vec{\theta}) \neq i^* . \quad (3)$$

As a distance metric for quantifying the perturbations of the input data $x_i^0 \in \vec{x}^0$, we use a squared L_2 norm of mean mean-squared deviations of perturbed feature values \vec{x}^a with respect to the original values \vec{x}^0 ,

$$\eta = \frac{1}{N} \sum_{i=1}^N \left(\frac{x_i^0 - x_i^a}{\sigma_i} \right)^2 . \quad (4)$$

The deviation of each feature is individually normalized to its uncertainty σ_i , similar to a χ^2 value in statistics, and the function is overall normalized to the dimension N of the input data. Note that this metric can be easily extended to correlated input features by using $(\vec{x}^0 - \vec{x}^a)^T \Sigma^{-1} (\vec{x}^0 - \vec{x}^a)$ where Σ is the covariance matrix.

Additionally, for our classification attack, we have to define a target score g for the attack. Here, we have two choices. Withoug loss of generality, assuming the target output of the class f_{i^*} approaches 1 for a very confident classification, a reverted classification corresponds to $f_{i^*}(\vec{x}^a; \vec{\theta}) = g$ with $g = 0$, or another desired score $g \neq f_{i^*}(\vec{x}^0; \vec{\theta})$. Note that this requirement does not restrict the possible values of the other $m-1$ classes $f_{i \neq i^*}$. Alternatively, one can explicitly set target scores $g_i \in \vec{g}$ for a subset or all output classes.

In the second case, the distance of a network output \vec{f} to the target score can then be defined by the L_2 metric similarly to the input metric Δ^2 with $\Delta = \vec{f}(\vec{x}^a; \vec{\theta}) - \vec{g}$. In our tests, we focus on the first variant of a changed classification without requiring a specific new label i or a specific output score for other labels $i \neq i^*$. For this case, the distance for the target score

simplifies to $(f_{i^*}(\vec{x}^a; \vec{\theta}) - g)^2$, where typically $g = 0$. This means we are targeting a maximal change of the initial classification without constraining the outputs for other classes. Obviously, also a mixed metric of the two alternatives, e.g., setting multiple output classes to zero, can be implemented, if conceptually required. For **MiniFool**, we now construct the total metric as

$$\lambda(\vec{x}^0; \vec{x}^a; \vec{\theta}) = \alpha \cdot \eta(\vec{x}^0; \vec{x}^a) + \beta \cdot (f_{i^*}(\vec{x}^a; \vec{\theta}) - g)^2 \quad (5)$$

where f_{i^*} depends on the perturbed input \vec{x}^a and the parameters $\vec{\theta}$ of the tested network. Optionally, α and β are normalizations that allow weighting the relative importance of the two distance terms. For each individual data event, this metric is minimized with respect to the adversarial perturbations to obtain our adversarial example \vec{x}_{min}^a

$$\vec{x}_{min}^a = \vec{x}^a \quad \text{for} \quad \arg \min_{\vec{x}^a} \lambda(\vec{x}^0; \vec{x}^a; \vec{\theta}) . \quad (6)$$

Depending on the values of the data uncertainties σ_i as well as the target score, an optimum solution is found for each individual event. If small perturbations can easily achieve the desired target score, the classification will be changed with minimal changes to the input, while if small perturbations cannot easily achieve the target, the optimum solution would favor not changing the initial classification.

The concept of a changed classification depending on the assumed uncertainty scale can be extended into a test that allows quantifying the robustness of the classification of the network for each individual event. In the simplest version, we scale the nominal uncertainties $\vec{\sigma}^0$ with a scalar parameter s which we call *attack parameter*

$$\vec{\sigma} = s \cdot \vec{\sigma}^0 \quad (7)$$

Here, $s = 1$ corresponds to the nominal uncertainties. Each individual data event can be scanned by evaluating the optimum classification score as a function of this attack parameter. A flipped classification only for $s \gg 1$ would indicate a robust classification, while a flipped classification for $s \leq 1$ signals a less robust classification.

MiniFool is available as both a TensorFlow [24, 25] and a PyTorch [26, 27] implementation. The minimization is computationally more demanding than many other adversarial algorithms. The execution time to create one adversarial example depends on the size of the image and network, as well as on the choice of the hyperparameters of the minimizer. It can take up to a few seconds on a typical workstation and is thus slower than other adversarial attack methods. The code of **MiniFool** is published as open source on GitHub [28]. A simple MNIST example is included to demonstrate its application.

4 Warm-up: Image Recognition with the MNIST Dataset

To illustrate the concept of the minimization-based adversarial attack in **MiniFool**, we apply it to the well-known MNIST digit classification task [14, 15]. MNIST consists of grayscale images of handwritten digits from 0 to 9, each of size 28×28 pixels. The input dimensionality is thus $N = 784$, and the number of classes is $m = 10$. We train a standard feedforward neural network illustrated in [Figure 1](#). The model is trained using cross-entropy loss and achieves over 98 % test accuracy. The trained model remains fixed throughout the adversarial attack process.

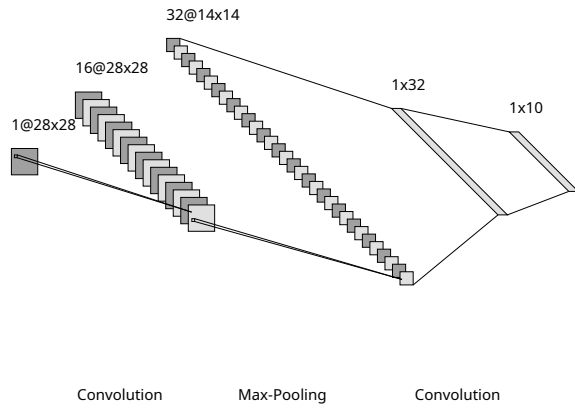


Figure 1 Simple network for the classification of MNIST images.

We apply the **MiniFool** attack to two images illustrated in [Figure 2](#). The first row shows an image of a "9" that is correctly classified as "9". After the **MiniFool** attack, it is classified as "4" with a softmax score of 93 % confidence, while the score for "9" is reduced to 6 %. The second row shows a true "9" that is wrongly classified as "8" with a score of almost 99 % while the score of the true label "9" is less than 1 %. After the attack, which only targets changing the "8" into something else, it is correctly classified as "9" with a score of 83 %, and the score for "8" is reduced to 16 %. The respective left plot shows the original, the center the attacked, and the right the difference between the two. All attacks were performed with an attack parameter $s = 0.2$ and $\sigma_i^0 = x_i^0$. During the attack, the image was not constrained to the original image's grayscale range. We observe that approximately 80 % of initially incorrectly classified images receive the correct label after the attack.

To further analyze the behavior of the attack, we applied **MiniFool** with varying attack parameters to two groups of test images: approximately 200 that were initially misclassified and another 200 that were

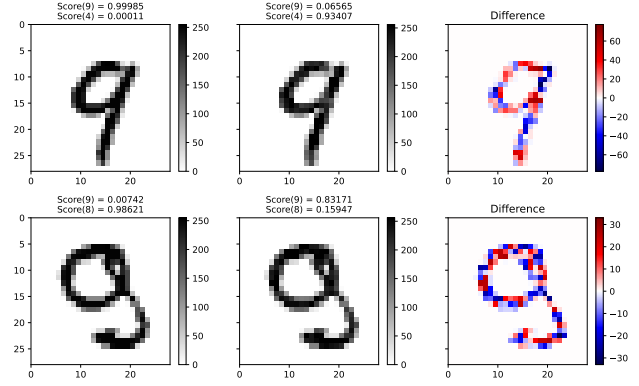


Figure 2 Example of **MiniFool** Attacks on MNIST images. The upper row shows a correctly and the bottom row a wrongly classified "9". The bottom row is wrongly classified as an "8". Left are the original images, the middle shows the images perturbed by **MiniFool** with an attack parameter $s = 0.2$. The right figures show the applied optimal perturbations. The respective classification scores can be seen above the images.

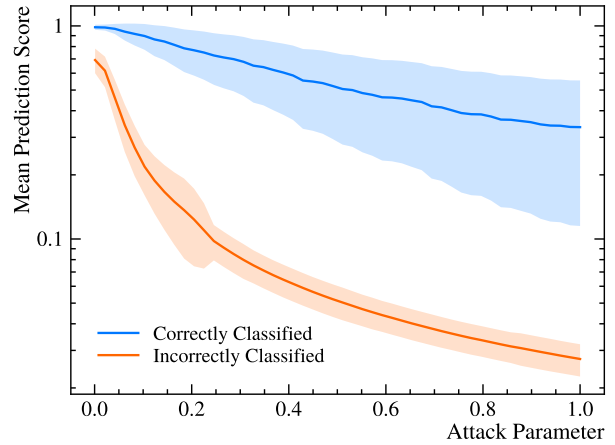


Figure 3 Average softmax score of the initially predicted class as a function of the attack parameter. The solid lines show the mean over correctly and incorrectly classified samples, while the shaded bands indicate one standard deviation. Misclassified samples exhibit a faster confidence decay under adversarial perturbation.

correctly classified. For each group, we tracked the softmax score of the originally predicted class as a function of the attack parameter. The results, shown in [Figure 3](#), display the average score of each image group with the standard deviation indicated as a shaded band. As expected, we observe a gradual decline in classification score with increasing attack strength. This decline is significantly smaller for correctly classified images, while the misclassified images show a much faster drop. This indicates that incorrect predictions are typically less robust to adversarial perturbations.

5 IceCube’s Tau Neutrino Analysis

The IceCube Neutrino Observatory [13] is a large ice-Cherenkov detector instrumenting roughly 1 km^3 (i.e. 1 Gton) natural deep ice at the geographical South Pole. It consists of 5160 optical sensors, called *DOMs*, on a hexagonal arrangement of 86 vertical cables, called *strings*, buried 1450 m to 2450 m below the ice surface. The main goal of IceCube is the measurement of neutrinos from astrophysical sources. Neutrino interactions inside or close to the detector result in Cherenkov light that is detected by the DOMs. Based on the number and arrival times of detected Cherenkov photons, the direction, energy, and flavor of the neutrino can be inferred, thus establishing an astronomical telescope.

In 2013 IceCube discovered a flux of high-energy neutrinos of astrophysical origin [29]. While IceCube is sensitive to all flavors of neutrinos, ν_e , ν_μ , and ν_τ , the latter tau neutrinos are particularly interesting as they are marginally produced in air showers at high energy and thus represent a unique signature of astrophysical origin [30]. However, the clear identification of tau neutrinos is challenging for that energy range, where most astrophysical neutrinos are detected in IceCube. Tau neutrinos need to be distinguished from the other neutrino flavors ν_e and ν_μ as well as from atmospheric muons, induced by cosmic-ray air showers, and require a challenging analysis and data selection [2, 30, 31]. Previous attempts to identify tau neutrinos within the recorded astrophysical neutrino events included dedicated searches for the distinct double-cascade signatures of tau neutrinos: *double bang* events [32], i.e. two separated energy depositions, or *double pulses* in raw waveforms of the DOMs and succeeded with a few candidates for ν_τ [30, 31]. In 2024, the observatory reported the evident observation of seven events with the signature of a tau neutrino interaction in the detector, in excess of the background expectation of 0.5 events [2]. This analysis employed a neural network-based approach utilizing standard image recognition techniques. Here, the recorded waveforms of the DOMs, i.e. the recorded voltage versus time (which reflects the sensor’s response to the arriving photons), are encoded as 2D images. Each image represents one of the vertical strings of 60 DOMs. The vertical axis represents the position number of the DOM along the string, which also corresponds to the depth of the sensor. The horizontal axis is the relative time of the recorded signals in that DOM, where each pixel corresponds to a time bin of 3.3 ns. The individual pixel values represent the measured amplitude of the waveform in units of photo-electrons. An example image is shown in Figure 4.

A central element of the data selection of the ν_τ search is based on several convolution networks with

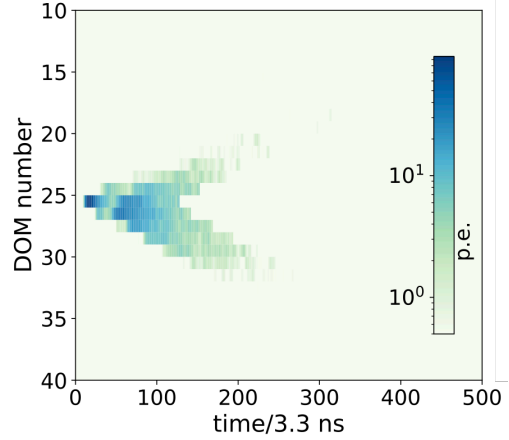


Figure 4 Example image of a recorded ν_τ candidate event, recorded in Nov. 2019. The image shows the data recorded by the DOMs on the string closest to the interaction vertex (leading string). The recorded DOM amplitude, normalized to photo-electrons, is represented as 60×500 pixel image corresponding to the sensor number (or depth, respectively) along the vertical axis and the time in steps of 3.3 ns on the horizontal axis. Clearly visible is the starting point of the event, and then the distance-dependent arrival of photons at the DOMs of the string. The total number of recorded photons is 6000. (modified picture taken from the supplementary material in [2])

standard VGG16 architecture [33] that are trained with labeled simulated data for the classification of different event types. Inputs to these networks are each three images, corresponding to the recorded data of those three strings that are located closest to the spatial interaction vertex within the detector. In the following, we will focus on the network that distinguishes ν_τ induced events from ν_e events, which are the most critical background in the analysis. The network’s output score ranges between 1 for likely ν_τ and 0 for likely ν_e induced events. More details of the analysis are found in [2].

For the application of **MiniFool**, we have chosen to attack only pixels with a non-zero recorded signal and assume the same relative uncertainty for all pixels proportional to the recorded amplitude of that pixel. Our default attack parameter is $s = 1$ with $\sigma_i^0 = 0.1 \cdot x_i^0$, which corresponds to an uncertainty of 10% of the respectively recorded amplitude in that pixel. For selected ν_τ candidates, the goal score becomes $g = 0$. More details of the implementation are given in [22].

The attack is illustrated in Figure 5, which shows a simulated ν_e event that was falsely classified as ν_τ with a score of $f(\vec{x}^0; \vec{\theta}) = 0.9907$ (top left). After the attack (top right), the score is reduced to $f(\vec{x}^a; \vec{\theta}) = 0.1413$. The difference between the two images $\vec{x}^0 - \vec{x}^a$ is shown on the bottom left. For the statistical quantification, we calculate the p-values where the applied changes are consistent with the uncertainty assumption (bottom right). This confidence calculation assumes a double-sided Gaussian distribution of width σ_i^0 for the calculation of the confidence interval of changes around

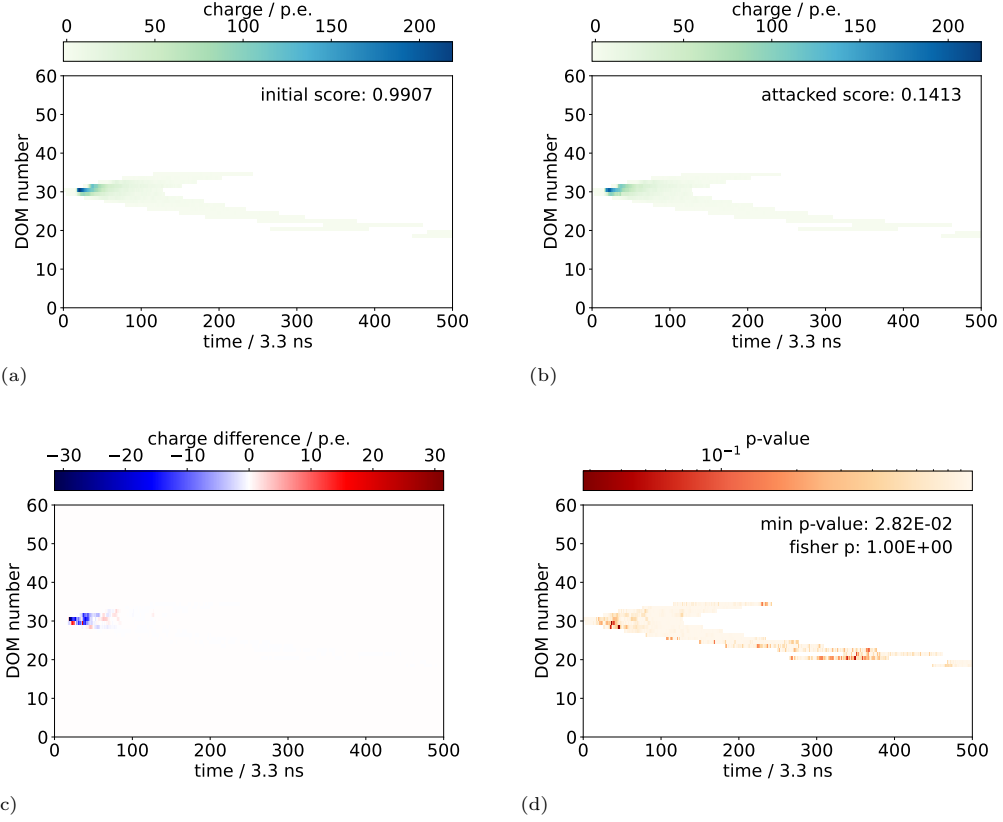


Figure 5 Example of an attack of a simulated IceCube event (modified images from [22]). (a) shows the original image of the measured charge versus time on the leading string. The image is attacked with `MiniFool` and an attack parameter of $s = 0.1$, resulting in (b). The difference (a)-(b) is shown in (c). Finally, (d) shows the p-value of applied changes.

the initial value x_i^0 . The smallest p-value is 2.8 % which corresponds to 2.2 standard deviations and is thus statistically acceptable given the large number of pixels. Also, the overall p-value that we obtain by combining all p-values with Fisher's method [34] is 1.

For the evaluation of the seven identified ν_τ candidate events in [2], we compare the application of `MiniFool` to these events with the expectation from simulated ν_τ and ν_e passing the final selection. The result of attacks is shown in Figure 6 as a function of the attack parameter s . For the default uncertainty $s = 1$, one of the seven events can be successfully attacked, resulting in a score of $f(\vec{x}^a; \vec{\theta}) \ll 1$ while for the remaining six events no solution with a changed classification is found and the score remains close to 1. When scanning the events as a function of the attack parameter, it is found that relatively small uncertainties $s < 1$ allow changing the classification for that one event, while the other six require substantially larger uncertainties of $s \approx 10$ (corresponding to the change in classification). Such large uncertainties of roughly $\sigma_i \simeq 100\% x_i$ are experimentally excluded. When comparing simulated events, we find that misclassified ν_e events are typically attackable with attack parameters of $s \lesssim 1$ similar to event 1, while correctly identified ν_τ events require larger values $s \gg 1$ similar to the

other six events. This observation is consistent with the background estimation in [2] of 0.5 events. As a result, we see that the robustness of the network decision can be quantified by scanning the attack parameter, and we see a clear distinction between misclassified and correctly classified events. This information can be exploited on the one hand as an independent verification of analysis results and estimated uncertainties that depend on classification tasks or even to improve the quality and purity of the data selection itself.

6 B-Jet Tagging with CMS Open Data

In order to test how generalizable the above findings are, we apply `MiniFool` to a very different test case in particle physics using data from the Compact Muon Solenoid (CMS) experiment [35, 36]. We consider a standard classification task, which is the identification of heavy quarks that are produced in particle collisions.

The CMS detector is a multi-purpose detector for electrons, muons, photons, and both charged and neutral hadrons that are produced in proton-proton or heavy-ion collisions at the CERN Large Hadron

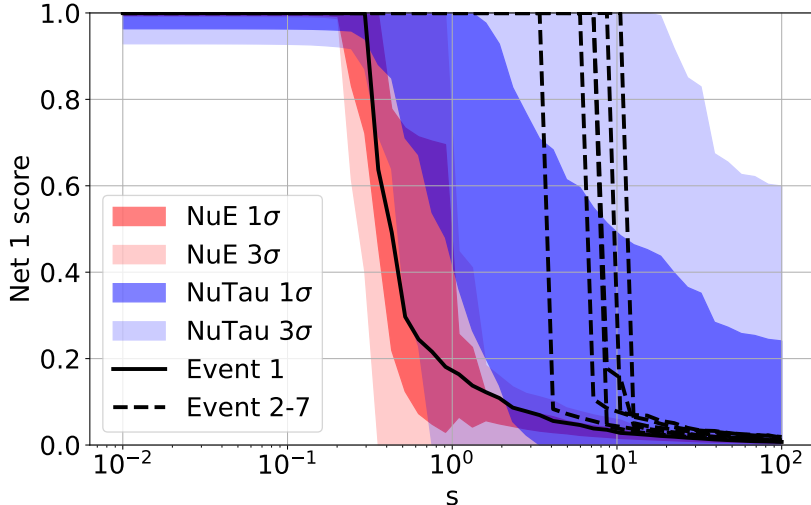


Figure 6 Network score versus attack parameter. The picture shows the resulting network scores for **MiniFool** attacks of the seven selected ν_τ candidates in [2] as black lines as a function of the assumed attack parameter s . For comparison the contours show the expectation of 68.3 % (dark) and 99.7 % central quantile range for simulated signal ν_τ events (blue) and background ν_e (red) events.

Collider (LHC). It uses a global particle-flow (PF) algorithm [37] to reconstruct all particles in an event. For this, data from multiple subsystems are combined: the tracking detectors, the electromagnetic and hadron calorimeters, and the muon detectors. The reconstructed particles are then used to reconstruct the global kinematics of the event. Here, so-called jets are reconstructed [38–40]. Jets are collimated sprays of particles that originate from the hadronization process of produced quarks and gluons [41].

The focus of our study is so-called b-tagging, which is the identification of jets induced by a b-quark and their separation from the background which consists of jets originating from lighter quarks and gluons. As input, we use a publicly available simulated event sample from the CMS open data portal [16]. The simulated events originate from top-quark pair decay into W bosons and b-quarks. The events are preselected for jet topologies and kinematic thresholds. These jets are identified (tagged) by DeepJet, which is a deep neural network that has been developed by the CMS Collaboration [42, 43]. Inputs to this network are more than 600 quantities from various sources. These quantities include global characterizing values of the jet, such as momentum, orientation, and the number of particle constituents. Furthermore, numerous low-level features for the individual constituents are included, e.g. relative geometrical and kinematic values. The included values are both floating point as well as integer numbers, such as the multiplicity of particles or simple flags such as identified photons. The output of DeepJet for each tested jet is the probabilities P for six different classes of jet-inducing particles. For this study, we compress this information into two classes: jets originating from b-quarks, denoted $P(B)$, and not from b-quarks,

$P(\bar{B})$. The dataset is fully labeled on the simulated truth information, allowing for supervised training of DeepJet. In total, 10 000 000 jets were used for training, split into 8 000 000 for the training and 2 000 000 for the validation step, respectively. The inference is performed on 1 000 000 jets. Normalization of the input data is handled by internal batch normalization layers in the model [44].

Prior to the application of **MiniFool**, we train DeepJet with the unperturbed dataset (nominal). To establish a baseline, we perform a nominal inference on the unperturbed test dataset. The performance is evaluated using a Receiver Operating Characteristic (ROC) curve [45, 46] that shows the sliding cut of a discriminator. Generally, a discriminator between classes X and Y is defined as

$$XvsY = \frac{P(X)}{P(X) + P(Y)}. \quad (8)$$

In our simplified case of two classes, we can identify $XvsY = BvsAll = P(B)$. To quantify the performance, the Area Under the Curve (AUC) is used as a measure¹. The nominal performance of the DeepJet model is shown by the black line in Figure 7, yielding an AUC of 0.932.

In the following, the impact of the **MiniFool** attack on the decision-making of our nominal-trained DeepJet model is studied. Each iteration is computationally expensive. Given the large size of the event samples, we perform **MiniFool** with only ten iterations on the full dataset. We aim to maximize the change in the initial

¹Note that we use the AUC convention of the CMS jet tagging group, where the used AUC is given by the area above the curve.

classification. For this purpose, we start from the total metric [Equation \(5\)](#), identify $g = 0$, $\alpha = \beta = 1$, and use the adapted L_2 metric in [Equation \(4\)](#) with

$$\sigma_i = a_i \cdot s. \quad (9)$$

The scaling variable a_i normalizes the inputs, while s is the attack parameter, as above. In contrast to the previous applications, the nominal uncertainties $\vec{\sigma}^0$ of the more than 600 different input quantities are difficult to quantify. For simplicity of this test case, it is generally set to unity and varied using one global attack parameter.

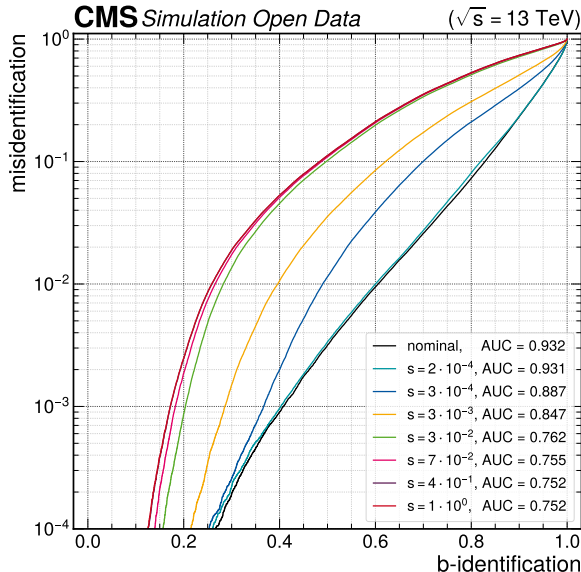


Figure 7 ROC curves for the jet-tagging performance for the full data set (see text). Shown is the nominally trained model and the results of perturbed data with different attack parameters.

The evaluation of DeepJet with perturbed inputs is shown in [Figure 7](#) for attack parameters of $\mathcal{O}(10^{-4}) - \mathcal{O}(10^0)$. While the performance of DeepJet with $s = 2 \times 10^{-4}$ recovers almost the nominal performance, the first degradation in performance can be observed for an attack parameter of 3×10^{-4} with a corresponding AUC of 0.887. Generating more severe input perturbations using higher attack parameters leads to more severe performance degradations. The additional degradations incurred beyond that caused by $s = 3 \times 10^{-2}$ are not as substantial as the degradations below. As expected for the proposed cost function, the dependency on s is highly non-linear. We show this by setting the attack parameter to unity, implying that the uncertainty is on the same order of magnitude as the input itself. Using this artificially high uncertainty, we can investigate the limit of degradation and find

a convergence to an AUC of 0.752. This leads to the conclusion that DeepJet is nearly very robust against perturbations of its inputs that are smaller than 0.02 % of the normalized inputs.

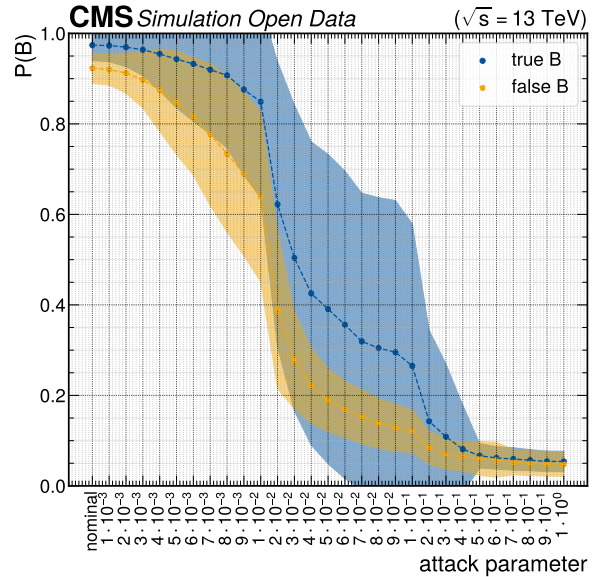


Figure 8 Network output as a function of the attack parameter s . The jets used here resemble a subset of the original test set (see text). By requiring an initial confidence of at least 87 %, we select 200 jets, split equally between correctly (blue) and incorrectly (orange) classified jets. The dotted curve shows the mean of the output $P(B)$, while the shaded region represents the corresponding standard deviation.

As a next study, we investigate 200 randomly selected jets of the class $P(B)$ which were classified with a confidence $P \geq 87\%$ by the nominal model. Out of these, half are chosen from correctly classified B jets (true), while the other half is misclassified as B (false). For these jets, we scan the robustness against the attack parameters s similar to the previous test cases. For each tested s , we ensure full convergence of `MiniFool` by allowing for up to 1000 iterations. [Figure 8](#) shows the result of the scan. For this subset of highly confident classification, we see the largest change in the classification shifted to larger attack parameters. Furthermore, we reproduce the findings of the previous test cases. Increasing s shows higher robustness for initially correctly classified jets compared to initially incorrectly classified ones, despite a similar high confidence of selected data.

7 Discussion

Adversarial attacks are being established as a powerful tool in the evaluation of physics analyses in the field of elementary particle and astroparticle physics.

However, as a challenge, typical algorithms for adversarial attacks do not preserve constraints imposed by physics unless supplemented by specific custom modifications. In this paper, we present the new algorithm `MiniFool` that combines experimental uncertainties with the goal of changing classifications by minimal adversarial perturbations of the input data. The algorithm is applied to individual events and optimizes the minimum change according to the uncertainty of the input data and the changed target score. Depending on the assumed uncertainties, the attacks are successful or unsuccessful in case the required changes to the input are too costly. We present three test cases: classification of MNIST numbers, identification of ν_τ in the IceCube Neutrino Observatory, and Classification of tagged jets in the CMS experiment. In all cases, we consistently find that the algorithm is capable of testing classifications of experimental data. Furthermore, it allows distinguishing between correctly classified and misclassified data by scanning the success of the attack as a function of the scale of the assumed uncertainty.

Looking ahead, we see that the inclusion of physical boundary conditions into an adversarial attack enhances the possibilities of quantitatively evaluating the result from such an attack. For future applications, more complex uncertainty models need to be applied to achieve a more realistic application of experimental constraints. While currently we have focused on testing decisions of pre-trained networks, the application within the training process also needs to be studied. However, here, the speed of the relatively slow numerical minimization process by the algorithm would currently limit the applicability to relatively small data samples. As a further future aspect, the question of applying a similar algorithm to regression tasks arises. Here, the metric of a target score needs to be replaced by a metric that describes a significant deviation from the original regression result.

Supplementary information.

Acknowledgements. We kindly acknowledge the permission to use simulated data from the IceCube and CMS Collaborations for this study. Particularly, we thank Doug Cowen for providing the classification network of IceCube’s ν_τ search. This work has been conducted within the context of the *AISafety* Project, that has been funded within the funding line *Software und Algorithmen zur Erforschung von Universum und Materie (ErUM) mit Schwerpunkt auf Künstlicher Intelligenz und Maschinellem Lernen* by the *Bundesministerium für Bildung und Forschung (BMBF)* of Germany.

Author contributions. The presented work has been developed as a collaborative effort by all authors within the *AISafety* Project. O.J., P.A.J., P.S.,

M.T., and U.W. have contributed to the implementation of the code. The manuscript has been prepared by O.J., P.A.J., P.S., C.W., and U.W.. All authors have reviewed and contributed to the manuscript.

Declarations. The authors declare no competing interests.

Code availability. The code is available as both a TensorFlow and a PyTorch implementation as open source on GitHub [28].

Data availability. The MNIST data set can be accessed through the used software packages TensorFlow and PyTorch. The CMS data is publicly available through the CERN Open data portal. [16]. The IceCube simulation data is scheduled for a data release through the IceCube portal for public data [47].

References

- [1] Erdmann, M., Glombitza, J., Kasieczka, G., Klemraadt, U.: Deep Learning for Physics Research, (2021). <https://doi.org/10.1142/12294>
- [2] The IceCube Collaboration: Observation of Seven Astrophysical Tau Neutrino Candidates with IceCube. *Phys. Rev. Lett.* **132**(15), 151001 (2024) <https://doi.org/10.1103/PhysRevLett.132.151001> arXiv:2403.02516 [astro-ph.HE]
- [3] The IceCube Collaboration: Observation of high-energy neutrinos from the Galactic plane. *Science* **380**(6652), 9818 (2023) <https://doi.org/10.1126/science.adc9818> arXiv:2307.04427 [astro-ph.HE]
- [4] The IceCube Collaboration: Evidence for neutrino emission from the nearby active galaxy NGC 1068. *Science* **378**(6619), 538–543 (2022) <https://doi.org/10.1126/science.abg3395> arXiv:2211.09972 [astro-ph.HE]
- [5] Pierre Auger Collaboration: Inference of the Mass Composition of Cosmic Rays with Energies from $10^{18.5}$ to 10^{20} eV Using the Pierre Auger Observatory and Deep Learning. *Phys. Rev. Lett.* **134**, 021001 (2025) <https://doi.org/10.1103/PhysRevLett.134.021001>
- [6] Hashemi, B., Hartmann, N., Sharifzadeh, S., Kahn, J., Kuhr, T.: Ultra-high-granularity detector simulation with intra-event aware generative adversarial network and self-supervised relational reasoning. *Nature Communications* **15**(1), 4916 (2024) <https://doi.org/10.1038/s41467-024-49104-4>
- [7] Lai, Y.S., Neill, D., Płoskoń, M., Ringer, F.: Explainable machine learning of the underlying

physics of high-energy particle collisions. *Physics Letters B* **829**, 137055 (2022) <https://doi.org/10.1016/j.physletb.2022.137055>

[8] Oliveira, L., Paganini, M., Nachman, B.: Learning Particle Physics by Example: Location-Aware Generative Adversarial Networks for Physics Synthesis. *Computing and Software for Big Science* **1**(1) (2017) <https://doi.org/10.1007/s41781-017-0004-6>

[9] Xu, H., Ma, Y., Liu, H.-C., Deb, D., Liu, H., Tang, J.-L., Jain, A.K.: Adversarial attacks and defenses in images, graphs and text: A review. *International journal of automation and computing* **17**, 151–178 (2020) <https://doi.org/10.1007/s11633-019-1211-x>

[10] Favereau, J., Delaere, C., Demin, P., Giannanco, A., Lemaître, V., Mertens, A., Selvaggi, M.: DELPHES 3, A modular framework for fast simulation of a generic collider experiment. *JHEP* **02**, 057 (2014) [https://doi.org/10.1007/JHEP02\(2014\)057](https://doi.org/10.1007/JHEP02(2014)057) [arXiv:1307.6346](https://arxiv.org/abs/1307.6346) [hep-ex]

[11] Carlini, N., Wagner, D.: Towards Evaluating the Robustness of Neural Networks. In: 2017 IEEE Symposium on Security and Privacy (SP), pp. 39–57 (2017). <https://doi.org/10.1109/SP.2017.49>

[12] Goodfellow, I.J., Shlens, J., Szegedy, C.: Explaining and Harnessing Adversarial Examples (2015) <https://doi.org/10.48550/arXiv.1412.6572> [arXiv:1412.6572](https://arxiv.org/abs/1412.6572) [stat.ML]

[13] The IceCube Collaboration: The IceCube Neutrino Observatory: Instrumentation and Online Systems. *JINST* **12**(03), 03012 (2017) <https://doi.org/10.1088/1748-0221/12/03/P03012> [arXiv:1612.05093](https://arxiv.org/abs/1612.05093) [astro-ph.IM]. [Erratum: *JINST* **19**, E05001 (2024)]

[14] LeCun, Y., Cortes, C., Burges, C.: MNIST handwritten digit database (2010). <http://yann.lecun.com/exdb/mnist>

[15] Deng, L.: The MNIST Database of Handwritten Digit Images for Machine Learning Research [Best of the Web]. *IEEE Signal Processing Magazine* **29**(6), 141–142 (2012) <https://doi.org/10.1109/MSP.2012.2211477>

[16] The CMS Collaboration: Simulated dataset TT-ToHadronic_TuneCP5_13TeV-powheg-pythia8 in MINIAODSIM format for 2016 collision data (2024) <https://doi.org/10.7483/OPENDATA.CMS.G6CE.1ITV> . [CERN Open Data Portal]

[17] Saala, T., Flek, L., Jung, A., Karimi, A., Schmidt, A., Schott, M., Soldin, P., Wiebusch, C.: Enforcing Fundamental Relations via Adversarial Attacks on Input Parameter Correlations (2025) <https://doi.org/10.48550/arXiv.2501.05588> [arXiv:2501.05588](https://arxiv.org/abs/2501.05588) [cs.LG]

[18] Stein, A.: Novel jet flavour tagging algorithms exploiting adversarial deep learning techniques with efficient computing methods and preparation of open data for robustness studies. Dissertation, RWTH Aachen University, Aachen (2024). <https://doi.org/10.18154/RWTH-2024-07840> . Veröffentlicht auf dem Publikationsserver der RWTH Aachen University; Dissertation, RWTH Aachen University, 2024

[19] Stein, A., Coubez, X., Mondal, S., Novak, A., Schmidt, A.: Improving Robustness of Jet Tagging Algorithms with Adversarial Training. *Comput. Softw. Big Sci.* **6**(1), 15 (2022) <https://doi.org/10.1007/s41781-022-00087-1> [arXiv:2203.13890](https://arxiv.org/abs/2203.13890) [physics.data-an]

[20] Madry, A., Makelov, A., Schmidt, L., Tsipras, D., Vladu, A.: Towards Deep Learning Models Resistant to Adversarial Attacks (2019) <https://doi.org/10.48550/arXiv.1706.06083> [arXiv:1706.06083](https://arxiv.org/abs/1706.06083) [stat.ML]

[21] Moosavi-Dezfooli, S.-M., Fawzi, A., Frossard, P.: DeepFool: A Simple and Accurate Method to Fool Deep Neural Networks. In: 2016 IEEE Conference on Computer Vision and Pattern Recognition (CVPR), pp. 2574–2582 (2016). <https://doi.org/10.1109/CVPR.2016.282>

[22] Janik, O.: Using Adversarial Attacks to Fool IceCube’s Deep Neural Networks. Master Thesis, RWTH Aachen University (2023). https://www.institut3b.physik.rwth-aachen.de/global/show_document.asp?id=aaaaaaaaacgjxigu

[23] Szegedy, C., Zaremba, W., Sutskever, I., Bruna, J., Erhan, D., Goodfellow, I., Fergus, R.: Intriguing properties of neural networks (2014) <https://doi.org/10.48550/arXiv.1312.6199> [arXiv:1312.6199](https://arxiv.org/abs/1312.6199) [cs.CV]

[24] Abadi, M., Barham, P., Chen, J., Chen, Z., Davis, A., Dean, J., Devin, M., Ghemawat, S., Irving, G., Isard, M., Kudlur, M., Levenberg, J., Monga, R., Moore, S., Murray, D.G., Steiner, B., Tucker, P., Vasudevan, V., Warden, P., Wicke, M., Yu, Y., Zheng, X.: TensorFlow: A system for large-scale machine learning (2016). <https://doi.org/10.48550/arXiv.1605.08695>

[25] Abadi, M., Agarwal, A., Barham, P., Brevdo, E., Chen, Z., Citro, C., Corrado, G.S., Davis, A., Dean, J., Devin, M., Ghemawat, S., Goodfellow, I., Harp, A., Irving, G., Isard, M., Jia, Y., Jozefowicz, R., Kaiser, L., Kudlur, M., Levenberg, J., Mané, D., Monga, R., Moore, S., Murray, D., Olah, C., Schuster, M., Shlens, J., Steiner, B., Sutskever, I., Talwar, K., Tucker, P., Vanhoucke, V., Vasudevan, V., Viégas, F., Vinyals, O., Warden, P., Wattenberg, M., Wicke, M., Yu, Y., Zheng, X.: TensorFlow: Large-Scale Machine Learning on Heterogeneous Systems. Software available from tensorflow.org (2015). <https://www.tensorflow.org/>

[26] Paszke, A., Gross, S., Massa, F., Lerer, A., Bradbury, J., Chanan, G., Killeen, T., Lin, Z., Gimelshein, N., Antiga, L., Desmaison, A., Köpf, A., Yang, E., DeVito, Z., Raison, M., Tejani, A., Chilamkurthy, S., Steiner, B., Fang, L., Bai, J., Chintala, S.: PyTorch: An Imperative Style, High-Performance Deep Learning Library (2019) <https://doi.org/10.48550/arXiv.1912.01703> [cs.LG]

[27] Paszke, A., Gross, S., Chintala, S., Chanan, G., Yang, E., DeVito, Z., Lin, Z., Desmaison, A., Antiga, L., Lerer, A.: Automatic differentiation in PyTorch (2017). <https://openreview.net/pdf?id=BJJsrmfCZ>

[28] Janik, O., et al.: MiniFool. GitHub repository (2025). <https://github.com/ojanik/MiniFool>

[29] The IceCube Collaboration: Evidence for High-Energy Extraterrestrial Neutrinos at the IceCube Detector. *Science* **342**, 1242856 (2013) <https://doi.org/10.1126/science.1242856> [arXiv:1311.5238](https://arxiv.org/abs/1311.5238) [astro-ph.HE]

[30] The IceCube Collaboration: Detection of astrophysical tau neutrino candidates in IceCube. *Eur. Phys. J. C* **82**(11), 1031 (2022) <https://doi.org/10.1140/epjc/s10052-022-10795-y> [arXiv:2011.03561](https://arxiv.org/abs/2011.03561) [hep-ex]

[31] The IceCube Collaboration: Search for Astrophysical Tau Neutrinos in Three Years of IceCube Data. *Phys. Rev. D* **93**(2), 022001 (2016) <https://doi.org/10.1103/PhysRevD.93.022001> [arXiv:1509.06212](https://arxiv.org/abs/1509.06212) [astro-ph.HE]

[32] Learned, J.G., Pakvasa, S.: Detecting tau-neutrino oscillations at PeV energies. *Astropart. Phys.* **3**, 267–274 (1995) [https://doi.org/10.1016/0927-6505\(94\)00043-3](https://doi.org/10.1016/0927-6505(94)00043-3) [arXiv:hep-ph/9405296](https://arxiv.org/abs/hep-ph/9405296)

[33] Simonyan, K., Zisserman, A.: Very Deep Convolutional Networks for Large-Scale Image Recognition (2015) <https://doi.org/10.48550/arXiv.1409.1556> [arXiv:1409.1556](https://arxiv.org/abs/1409.1556) [cs.CV]

[34] Mosteller, F.: Questions and Answers. *The American Statistician* **2**(5), 30–31 (1948) <https://doi.org/10.1080/00031305.1948.10483405>

[35] The CMS Collaboration: The CMS Experiment at the CERN LHC. *JINST* **3**, 08004 (2008) <https://doi.org/10.1088/1748-0221/3/08/S08004>

[36] The CMS Collaboration: Development of the CMS detector for the CERN LHC Run 3. *JINST* **19**, 05064 (2024) <https://doi.org/10.1088/1748-0221/19/05/P05064>

[37] The CMS Collaboration: Particle-flow reconstruction and global event description with the CMS detector. *Journal of Instrumentation* **12**(10), 10003 (2017) <https://doi.org/10.1088/1748-0221/12/10/P10003>

[38] Cacciari, M., Salam, G.P., Soyez, G.: The anti- k_t jet clustering algorithm. *Journal of High Energy Physics* **2008**(04), 063–063 (2008) <https://doi.org/10.1088/1126-6708/2008/04/063>

[39] Ellis, S.D., Soper, D.E.: Successive combination jet algorithm for hadron collisions. *Physical Review D* **48**(7), 3160–3166 (1993) <https://doi.org/10.1103/physrevd.48.3160>

[40] Catani, S., Dokshitzer, Y.L., Seymour, M.H., Webber, B.R.: Longitudinally-invariant k_\perp -clustering algorithms for hadron-hadron collisions. *Nuclear Physics B* **406**(1), 187–224 (1993) [https://doi.org/10.1016/0550-3213\(93\)90166-M](https://doi.org/10.1016/0550-3213(93)90166-M)

[41] Rabbertz, K.: Jet Physics at the LHC: The Strong Force Beyond the TeV Scale. Springer Tracts in Modern Physics, vol. 268. Springer Cham, ??? (2017). <https://doi.org/10.1007/978-3-319-42115-5>

[42] Bols, E., Kieseler, J., Verzetti, M., Stoye, M., Stakia, A.: Jet flavour classification using DeepJet. *Journal of Instrumentation* **15**(12), 12012 (2020) <https://doi.org/10.1088/1748-0221/15/12/p12012>

[43] DL4Jets: DeepJet: Repository for training and evaluation of deep neural networks for jet identification. [Accessed: 02.09.2025] (2020). <https://github.com/DL4Jets/DeepJet>

- [44] Ioffe, S., Szegedy, C.: Batch Normalization: Accelerating Deep Network Training by Reducing Internal Covariate Shift (2015). <https://doi.org/10.48550/arXiv.1502.03167>
- [45] Bradley, A.P.: The use of the area under the ROC curve in the evaluation of machine learning algorithms. *Pattern Recognition* **30**(7), 1145–1159 (1997) [https://doi.org/10.1016/S0031-3203\(96\)00142-2](https://doi.org/10.1016/S0031-3203(96)00142-2)
- [46] Fawcett, T.: An introduction to ROC analysis. *Pattern Recognition Letters* **27**(8), 861–874 (2006) <https://doi.org/10.1016/j.patrec.2005.10.010>. ROC Analysis in Pattern Recognition
- [47] The IceCube Collaboration: Data Releases. IceCube portal for public data releases. <https://icecube.wisc.edu/science/data-releases/>